IV. Conclusions

The following conclusions were drawn from this study.

1) Flow behind a cylinder can be effectively influenced by a rear stagnation jet. The computational results are in good agreement with the experimental flow visualization.

2) The unsymmetric wake flow becomes symmetric when the rear stagnation jet is in operation with a velocity ratio as low as 1. The size of the symmetric recirculation region becomes smaller as the jet speed increases.

3) A rear stagnation jet forces a symmetrical wake flow pattern, thus eliminating the lateral force.

4) The pressure on the cylinder surface decreases over the entire surface, but significantly more on the downstream side of the cylinder, as the jet velocity increases, causing an increase in form drag as jet velocity ratio increases.

5) The rear stagnation jet to significantly increase form drag on a bluff body has direct applications in aerodynamic controls of reentry or flights at high angles of attack.

References

[1]Duke, M. R., Jr., "Effects of a Rear Stagnation Jet on the Wake Flow Behind a Cylinder," M.S. Thesis, Dept. of Mechanical Engineering, Memphis State Univ., Memphis, TN, Dec. 1992.

[2]Duke, R., Shrader, B., and Mo, J., "Effects of a Rear Stagnation Jet on the Wake Behind a Cylinder," *AIAA Journal*, Vol. 31, No. 9, 1993, pp. 1727–1729.

Surface Interference in Rayleigh Scattering Measurements near Forebodies

Zaidi B. Zakaria* and Steven H. Collicott†
Purdue University, West Lafayette, Indiana 47907

I. Introduction

HIGH-SPEED boundary-layer transition on forebodies is currently a topic of considerable interest.[1] Transition experiments in quiet-flow supersonic facilities[2] require nonintrusive diagnostics. Some form of Rayleigh scattering measurement is desirable in these flows because calibrated hot-wire measurements are elusive.[3] Rayleigh scattering measurements of density are feasible in various fluid flow experiments.[4–6] The simplest and least expensive method is to detect the scattered light without any spectral filtering. This permits use of an Nd:YAG laser without injection seeding. Thus if direct (unfiltered) Rayleigh scattering may be used rather than filtering the Doppler-shifted scattered light from an extremely stable narrow-band laser, considerable costs savings may be had.

Direct Rayleigh scattering is known to not be feasible near surfaces. Numerous flows of interest, such as boundary layers and the region between a blunt body and a bow shock, are near the surface. Thus experiments to quantify this near-body limit on forebodies are performed. The distance from the forebody within which one is forced to use a filtered Rayleigh technique must be known for proper experiment design. The question of how close to the forebody is too close is addressed by this experiment.

II. Theoretical Background

The energy per unit of solid angle of the light scattered by gas molecules in the direction perpendicular to the incident beam and its polarization vector is[7]

$$E_s = E_0 \sigma_s (3NV/8\pi) \tag{1}$$

where E_0 is the incident areal energy density, σ_s is the scattering cross section of the gas molecules, N is the number density of the gas, and V is the measurement volume in the gas. The total scattered energy, for optics collecting scattered light within a solid angle of $\Omega \ll 4\pi$, is then approximately

$$E_t = E_0 \sigma_s (3NV/8\pi)\Omega \tag{2}$$

Furthermore, since the number density of the gas is $N = \rho/m$, where ρ is the density of the gas and m is the mass of the gas per molecule, Eq. (2) can be written as

$$E_t = (3/8\pi)(\rho/m)V\Omega\sigma_s E_0 \tag{3}$$

To calculate the scattering volume, the incident beam is assumed to have a Gaussian distribution. Furthermore, since the radius of the pinhole on the photomultiplier tube (PMT) is larger than the image of the beam waist, a cylindrical volume is assumed. The cylinder has a circular area with the radius of the beam waist and a length equal to the diameter of the area captured by the PMT. Thus, the scattering volume V for the experiment is

$$V = [d_p/M_c][\lambda_f/w]^2 \tag{4}$$

where d_p is the diameter of the pinhole of the PMT, M_c is the magnification of the collection optics, λ is the wavelength of the laser, f is the focal length of the focusing lens, and w is the radius of the incident beam incident on the focusing lens.

III. Experiment Description

The geometry and components of the experiment are shown schematically in Fig. 1. A Q-switched frequency doubled Nd:YAG laser produced the beam that is focused by a lens (focal length = 100 mm). A low-speed (≈1 m/s) jet of nitrogen is allowed to flow through the focal volume. The nitrogen is used to minimize the presence of dust particles that would scatter more efficiently and obscure the Rayleigh scattered light. A sample of the beam is detected by an energy meter to determine the energy of the incident beam, whereas the scattered energy is imaged perpendicularly onto the PMT. Because of the need for uninterrupted propagation on both sides of the beam waist, the geometry described is probably not a good candidate for use over winglike surfaces. A tight stack of razor blades is stacked behind the jet to provide a nonreflecting background. The oscilloscope is trigged by the Nd:YAG so that there is reliable detection.

Following calibration of the PMT, light scattered from room temperature and pressure nitrogen is measured to insure that Rayleigh scattering is detected by the experiment. Approximately 10^{-15} J from a 0.1-J laser pulse is collected. This corresponds to an average power incident on the PMT of approximately 0.1μW during the duration of the 10-ns pulse. The observed signal is within 15% of the expected value calculated with the assumed cylindrical scattering volume. The error is primarily due to the assumption that the beam exhibited a Gaussian distribution, whereas physically the transverse mode structure of the Nd:YAG beam is complex. Because the scattering volume V is identical for every measurement in this experiment, and the results are normalized, the error in V does not affect the results. That is, the results are a measure of scattering per volume, independent of how accurately that volume is computed. Of course, if the data presented later had been acquired from different scattering spots, this would not be true. Application of these measurements to other beam waist sizes can be made by scaling with the Gaussian beam radius. Recall that the purpose of this experiment is to provide general data for experiment design and evaluation of the relative merits of various techniques, not to determine the minimum separation for a specific laser spot or aerodynamic model.

Nine different cylinders are used as representative test models. The surfaces of the nine bodies are in three categories: unpolished, polished, and painted flat black over a polished surface. In each category, there is a "thin" body (diameter = 4 mm), a "medium" body (diameter = 8 mm), and a "thick" body (diameter = 13 mm).

Received Aug. 9, 1993; revision received Oct. 25, 1993; accepted for publication Oct. 26, 1993.

*Student Research Assistant, School of Aeronautics and Astronautics.
†Assistant Professor, School of Aeronautics and Astronautics.

Each body is initially placed with the surface at the focal volume. The body is then moved away from the focal volume in the direction parallel to the axis of the collection optics (see Fig. 1) so that any reflection may be detected by the PMT. Signal measurements are recorded at intervals until the signal returns to expected Rayleigh scattering signal.

IV. Results

The results of the experiment are shown graphically on several figures. In each of the figures, the ordinate is the measured signal normalized by the theoretical Rayleigh scattering signal, and the abscissa is the distance between the surface of the body and the center of the focal volume, normalized by the radius of the body. The focusing lens has a focal length of 100 mm, which focuses the 4-mm radius raw incident beam to a beam waist with radius of approximately 14 μm.

Figure 2 is a plot of the data from the unpolished and polished bodies. The trend in this data is that as the diameter of the forebody increases, the normalized minimum separation for direct Rayleigh scattering measurements decreases. Data from the polished bodies have noticeably less spread than data from the unpolished bodies. This is attributed to the greater uniformity of the surfaces of the polished forebodies.

Figure 3 shows the data from the three bodies painted flat black following a polishing process. Note that the trend of minimum separation vs body radius is reversed relative to the unpolished and polished bodies. That is, the smallest diameter body has the smallest minimum separation for feasible direct Rayleigh scattering. The black surface has greater absorbence than either of the other surfaces, and perhaps this leads to a reduction of multiple reflections. In terms of non-normalized distances, the successful measurements closest to any body were made 2 mm from the 4-mm diameter blackbody.

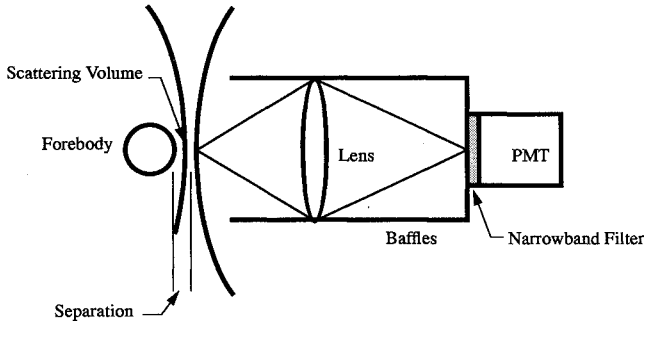

Fig. 1 Experiment setup; the separation of the body and the measurement volume is measured in the direction of the axis of the collection optics.

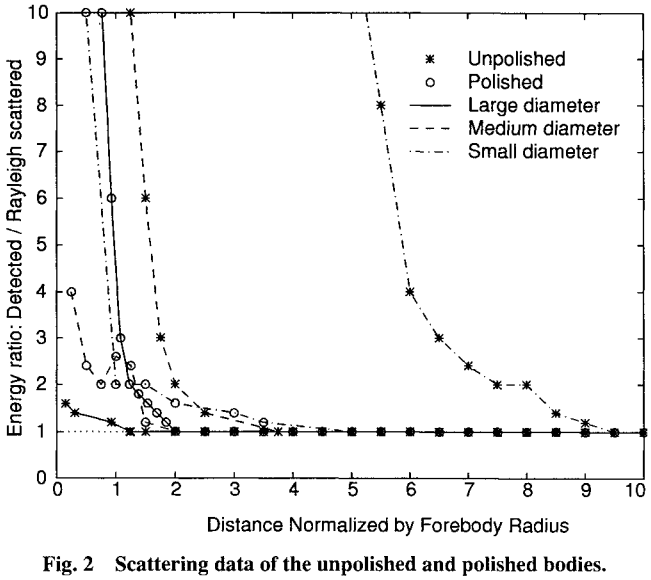

Fig. 2 Scattering data of the unpolished and polished bodies.

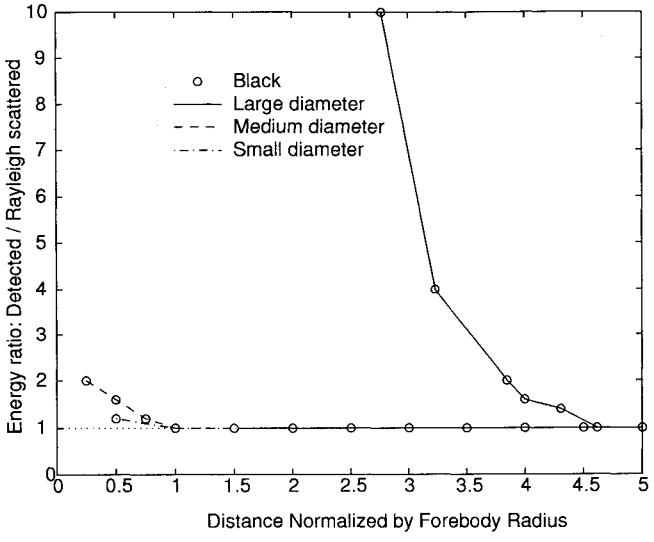

Fig. 3 Scattering data of the black painted bodies; common flat black spray paint is applied to the polished bodies.

V. Conclusions

The closest proximity for use of direct Rayleigh scattering near representative aerodynamic forebodies is determined. The purpose of the experiment is to provide data that will serve as guidelines for selection of nonintrusive diagnostic methods for experiments in high-speed forebody flows. The data presented quantify the near-body limits of the simplest form of Rayleigh scattering measurements. This experiment uses typical geometry and length scales for forebody flows in small supersonic tunnels.

The minimum separation, normalized by body radius, shows a different trend when for painted and unpainted bodies. For the unpainted bodies (polished and unpolished) increasing body size decreases the normalized minimum separation. Black painted bodies show the opposite trend. The minimum separation between the 14-μm beam waist and the bodies tested is found to be 2 mm. This is for a body diameter of 4 mm, flat black paint over polished aluminum, and pure nitrogen at room temperature and pressure.

The data suggest that the exact value of the minimum separation of the Rayleigh scattering volume and the aerodynamic model is not a simple relation. Length scales in the problem include optical wavelength, roughness, beam waist, model diameter, and perhaps streamwise radius of curvature. Rayleigh scattering is so weak relative to surface scattering that multiple-surface reflections strong enough to obscure the Rayleigh signal cannot all be prevented from entering the collection optics. The transverse mode structure of a high-energy Nd:YAG laser is a complex profile characteristic of the unstable resonator. This causes the minimum separation to differ for different lasers. Regardless, even the first significant figure of the previous results is a valuable design guideline for the distance within which a filtered Rayleigh scattering method must be used.

References

[1]Reed, H. L., and Haynes, T. S., "Transition Correlations in 3-D Boundary Layers," AIAA Paper 93-3054, July 1993.

[2]Schneider, S. P., "A Quiet-Flow Ludweig Tube for Experimental Study of High Speed Boundary Layer Transition," AIAA Paper 91-5026, Dec. 1991.

[3]Stainback, P. C., and Nagabushana, K. A., "Review of Hot-Wire Anemometry and the Range of Their Applicability," *Thermal Anemometry 1993*, ASME FED-Vol 167, American Society of Mechanical Engineers, New York, 1993.

[4]Miles, R. B., Forkey, J. N., and Lembert, W. R., "Filtered Rayleigh Scattering Measurements in Supersonic/Hypersonic Facilities," AIAA Paper 92-3894, July 1992.

[5]Shirinzadeh, B., Hillard, M. E., Balla, R. J., Waitz, I. A., Anders, J. B., and Exton, R. J., "Planar Rayleigh Scattering Results in Helium-Air Mixing Experiments in a Mach-6 Wind Tunnel," *Applied Optics*, Vol. 31, 1992, pp. 6529–6534.

[6]Dowling, D. R., "Mixing in Gas Phase Turbulent Jets," Ph.D. Thesis, Graduate Aeronautical Labs., California Inst. of Technology, Pasadena, CA, 1988.

[7]Chopra, P., and Heddle, D., "Polarization Free Measurements of Rayleigh Scattering of Lyman-α," *Journal of Applied Physics: Atomic and Molecular Physics*, Vol. 7, 1974, pp. 2421–2428.

Shear Buckling Response of Tailored Composite Plates

Sherrill B. Biggers* and Stephane S. Pageau†
Clemson University, Clemson, South Carolina 29634

Introduction

BUCKLING is frequently an important consideration in the design of aerospace and other types of structures composed of thin, plate elements. A number of authors[1–7] have addressed optimization of composite plates for buckling resistance by adjusting the design variables (fiber orientations, ply thicknesses) uniformly across the planform of the plate. However, additional aspects of tailoring can easily be exploited with composite materials to further improve buckling response. These include the variation of fiber orientation angles over the planform of the plate[8,9] and the piecewise-uniform redistribution of materials with fixed fiber orientations across the planform.[10,11] Plates tailored in these two ways have membrane and bending stiffnesses that are not uniform over the planform of the plate. These nonuniform properties can interact and can increase buckling loads with no increase in the weight of the plate. Average membrane properties are affected by the variable fiber orientation approach but they are not significantly affected by piecewise-uniform tailoring. Furthermore, with this latter approach, compressive buckling load increases up to 200% have been shown compared to uniform plates.[10,11]

This Note evaluates the piecewise-uniform approach to tailoring as a means of improving the shear buckling loads of composite plates. This design approach is referred to herein as stiffness tailoring or, more simply, as tailoring. The primary objectives are to determine the tailoring patterns and the degree of concentration of the material used to achieve the tailoring in each pattern that maximize the shear buckling load and to quantify the maximum relative improvement that can be achieved in the buckling load compared to uniform plates.

Tailoring Approach

The plate to be tailored is assumed to be flat and supported on all four sides by substructure. Furthermore, the plate is considered to be a typical element in an assembly with similar plates adjacent to each side. In an aircraft structure, for example, the plate could represent a portion of the wing skin or a large-radius fuselage skin supported on its four sides by ribs, frames, spars, or stringers. The tailoring concepts investigated include diagonal patterns which are doubly symmetric with respect to the in-plane vertical and horizontal directions so that the sign of the shear load is inconsequential. In addition, only those concepts which permit all fibers to be continuous across the plate and between adjacent plates are considered.

Figure 1 illustrates two typical acceptable tailoring patterns and two unacceptable ones. In this figure, the darker areas are regions to which material has been relocated and are therefore thicker and stiffer than the lighter areas. Diagonal bands represent areas to which +45 or −45 deg material has been redistributed. With these restrictions on the tailoring geometry, all laminae are continuous in their fiber directions and no stress concentrations associated with fiber drop-off in the fiber direction are present. Local stress concentrations due to fiber joggles will, however, be present. These local stress concentrations are the subject of ongoing work but are not considered in this study. Fiber joggles could be minimized or eliminated if lightweight core material were added in the thinner regions to create a tailored sandwich plate. Results for tailored sandwich concepts are to be presented elsewhere. Simple schematics of possible geometries are shown in Fig. 2. Notice that these configurations have varying degrees of fiber joggles and have one or two flat external surfaces. All of the results reported herein correspond to concepts that have a flat midplane and laminates that are symmetric through the thickness relative to the midplane.

Finite Element Model

Buckling loads are computed for uniform and tailored plates using the ABAQUS finite element code.[12] Pure in-plane shear deformation is applied to the plate edges which, for compatibility with adjacent plates in an actual structure, are required to remain straight. Both positive and negative eigenvalues, corresponding to positive and negative applied shear loading, are computed. The eigenvalue with the lowest absolute value is taken as the critical buckling load. The elements chosen for the analysis are the eight-node quadrilateral anisotropic shear deformable (first-order shear theory) shell elements denoted S8R5 in the ABAQUS code. In some cases, the quadrilateral elements are degenerated to triangular elements. The relatively low transverse shear stiffness of composite materials can significantly affect the buckling loads of composite plates. This effect of transverse shear deformation becomes increasingly negative in regions where the plate thickness is increased due to tailoring. As a result, transverse shear deformation has a greater influence on the buckling loads of tailored plates than uniform plates[10] and must be included in the evaluation so that the benefits of tailoring are not overestimated. Model refinement needed to yield buckling loads within about 1% of converged values was determined for selected highly tailored cases. This level of refinement was used in generating the results shown herein.

Material Properties

Material properties representative of an intermediate modulus fiber, toughened resin composite (IM7/8551-7) are used. The following relative properties are taken from Dow[13]: $E_{11}/E_{22} = 13.90$, $G_{12}/E_{22} = 0.48$, and $\nu_{12} = 0.33$

Values for G_{13} and ν_{13} are assumed equal to G_{12} and ν_{12}, respectively. A value for G_{23} was calculated from micromechanics using the fiber volume fraction from Dow[13] and manufacturer's data for the shear stiffnesses of the matrix and the fiber. The resulting relative transverse shear modulus is $G_{23}/E_{22} = 0.305$.

Parametric Study

The baseline plate used for comparison in this study is a uniform, quasi-isotropic, 16-ply laminate with layup $[\pm 45/0/90]_{2s}$ and a width-to-thickness ratio of 100. Based on results for compressive buckling,[10] the effect of transverse shear deformations for this thin plate should be negligible for the uniform plate and on the order of 3–5% for the tailored plates. However, these effects are included in the reported results regardless of their magnitude. The primary design variables are the basic pattern of the tailoring and the degree to which material is redistributed in these patterns. The latter is quantified by a width ratio $\bar{b}$ defined as the total width b_1 of the stiffened regions (the darkened regions in Fig. 1) measured along a ±45-deg line divided by the total width $\sqrt{2}\,b$ along the diagonal.

The shear buckling loads for the tailored plates are reported as normalized buckling loads $\bar{N}_{xy}$ where the buckling load of the uniform baseline plate is used as the normalizing factor. Because of the variation of stiffness across the tailored plates and the imposition of uniform shear deformation, the shear loads on the edges of

Received Feb. 11, 1993; presented as Paper 93-1408 at the AIAA/ASME/ASCE/AHS/ASC 34th Structures, Structural Dynamics, and Materials Conference, La Jolla, CA, April 19–21, 1993; revision received Aug. 20, 1993; accepted for publication Sept. 2, 1993.

*Associate Professor, Department of Mechanical Engineering. Senior Member AIAA.

†Research Assistant, Department of Mechanical Engineering.